scientific reports

Check for updates

OPEN

EGCG activates Keap1/P62/Nrf2 pathway, inhibits iron deposition and apoptosis in rats with cerebral hemorrhage

Liang Hao[1,2,4], Aobo Zhang[1,4], Dongsheng Lv[3], LuLu Cong[1], Zhimin Sun[2] & Liqiang Liu[1]✉

Intracerebral hemorrhage (ICH) is a common cerebrovascular disease characterized by a high incidence, disability rate, and mortality. Epigallocatechin gallate (EGCG), a key catechin compound found in green tea, has received increasing attention for its potential neuroprotective and therapeutic effects in neurological disorders. Studies have indicated that EGCG may influence various signaling pathways and molecular targets, including the inhibition of oxidative stress, reduction of inflammatory responses, suppression of cell apoptosis, regulation of cell survival, and enhancement of autophagy. Although the exact mechanism of action of EGCG is not fully understood, it has become a focal point of research in various disciplines due to its promising potential. This study aims to investigate the effects of EGCG on oxidative stress, iron deposition, and cell apoptosis in rats with ICH, as well as to uncover the underlying mechanisms. An ICH rat model was created to simulate cerebral hemorrhage, while an in vitro model utilizing primary cortical neurons was developed. The neurons were pre-treated with EGCG before being exposed to Erastin and RSL3 to induce iron death. The levels of oxidative stress, iron deposition, and cell apoptosis were evaluated in both models. In the ICH model, EGCG was discovered to enhance the activation of the Keap1/P62/Nrf2 signaling pathway in both in vivo and in vitro studies. Furthermore, EGCG significantly elevated the levels of GPX4 and XCT proteins, as well as the nuclear expression of Nrf2. It was noted that the Nrf2 inhibitor ML385 partially decreased the expression of these proteins. Through the activation of the Keap1/P62/Nrf2 pathway, EGCG inhibits inflammation, oxidative stress and iron deposition in rats with cerebral hemorrhage. EGCG inhibits oxidative stress, iron deposition and apoptosis in rats with ICH by activating Keap1/P62/Nrf2 pathway.

Keywords EGCG, Intracerebral hemorrhage, Ferroptosis, Oxidative stress, Cell apoptosis

Abbreviations

ICH	Intracerebral hemorrhage
ROS	Reactive oxygen species
HE	Hematoxylin and eosin
CCK8	Cell Counting Kit-8
FPT	The Forelimb Placing Test
FPT	Corner Turn Test
TEM	Transmission Electron Microscopy
FJC	Fluoro-Jade C
MDA	Malondialdehyde
GSH	Glutathione

ICH is bleeding caused by blood vessel rupture within the brain, often linked to conditions such as hypertension and ruptured aneurysms. This serious neurological condition often results in brain tissue damage and functional impairment[1,2]. Despite advancements in surgical hematoma evacuation, the prognosis for ICH remains suboptimal, mainly due to primary and secondary injury[3]. Primary injury involves tissue damage, increased

[1]Department of Neurosurgery, The Second Hospital of Hebei Medical University, Shijiazhuang 050000, Hebei, China. [2]Department of Neurosurgery, The Third Hospital of Shijiazhuang, Shijiazhuang 050000, Hebei, China. [3]Department of Neurosurgery, The Fourth Hospital of Hebei Medical University, Shijiazhuang 050000, Hebei, China. [4]Liang Hao and Aobo Zhang contributed equally to this work. ✉email: 27400950@hebmu.edu.cn

intracranial pressure, and edema due to blood leakage. On the other hand, secondary injury is characterized by vascular neurotoxicity, cellular oxidative stress, and an inflammatory response triggered by substances like hemoglobin, heme, and iron[4].

EGCG, the primary polyphenolic compound found in tea leaves, is responsible for the beneficial effects on health. Its structure consists of two trihydroxyphenyl groups, giving it strong antioxidant properties[5]. Studies conducted in a laboratory setting have demonstrated EGCG's ability to scavenge free radicals[6,7]. The antioxidant capabilities of EGCG imply that the nearby hydroxyl groups on the B ring and the galloyl moiety in the C ring are the sites that directly interact with oxygen free radicals[8]. Conversely, oxidative stress mainly arises from reactive oxygen species (ROS), ultimately resulting in inflammation. A growing body of research suggests that EGCG exhibits anti-inflammatory and anti-apoptotic properties when dealing with neuronal oxidative stress[9,10]. Studies indicate that EGCG can enhance the survival rate of hippocampal neural stem cells and provide antioxidant benefits following LPS-induced inflammation in mice[11,12]. The neuroprotective properties of EGCG in neurodegenerative conditions are linked to its ability to potentially inhibit the activation of brain glial cells[13,14].

Iron deposition, a form of non-apoptotic programmed cell death that relies on iron, is becoming a promising target for treating iron-related cell death[15]. There is substantial evidence linking iron deposition to various pathological conditions such as cancer, stroke, traumatic brain injury, and neurodegenerative diseases[16]. In cases of ICH, iron deposition plays a significant role in causing tissue damage[17]. After ICH, hemoglobin/heme released from dissolved red blood cells is converted into ferrous ions by microglia and macrophages, leading to the production of reactive oxygen species and lipid peroxidation near the blood clot[18]. Microglia worsen the damage by releasing ferrous ions through the Fenton reaction, resulting in the creation of highly toxic hydroxyl radicals that harm cellular components and eventually cause neuronal death[19–23]. Despite the use of Ferrostatin-1 (FER-1) as a specific inhibitor of iron deposition, its clinical application is limited due to its instability in vivo[24,25]. Consequently, current research is focused on identifying a more stable and effective inhibitor of iron deposition.

Elucidating the precise neuroprotective mechanisms of EGCG is crucial. While there is a lack of reports on the role of EGCG in the ICH model, this study shows that EGCG can inhibition of oxidative stress, reduce iron deposition, and decrease cell apoptosis in rats with ICH by activating the Keap1/P62/Nrf2 pathway. The research aims to provide new therapeutic strategies for addressing iron-induced cell death and apoptosis associated with cerebral hemorrhage.

Materials and methods

Primary cortical neuronal cultures

On the 18th day of pregnancy, female rats were anesthetized with isoflurane and sterilized with 75% ethanol. An incision was made in the abdomen to remove brain tissue from the rat on ice. The fetal rat's bilateral cerebral cortices were isolated and membranes removed. The meninges were removed and transferred to 1 mL of Hank's balanced salt solution on ice, where they were chopped and digested with trypsin (BD Biosciences, USA). The digestion was terminated with DMEM medium (Gibco, USA) containing 10% fetal bovine serum (Gibco, USA). Cells were inoculated into six-well plates coated with a cell adherent reagent (APPLYGEN, China). Neurobasal medium supplemented with 2% B27, 1% l-glutamine, and a Mycoplasma prevention reagent was maintained at 37 °C in a 5% CO2 atmosphere. The medium should be replaced every three days.

In vitro ICH model and drug therapy

Cultured neurons were exposed to Hemin (20μM; Sigma-Aldrich) to mimic hemorrhagic stroke. Ferroptosis was triggered in cultured neurons using Erastin (2.5μM, MedChemExpress, USA) and RSL3 (1μM, MedChemExpress, USA). The control group cells were treated with DMEM medium without FBS. EGCG (MCE, USA, purity: 99.75%, C22H18O11) was co-administered at varying concentrations (5 μM-20 μM) in DMEM medium along with Hemin (20μM; Sigma-Aldrich). Fer-1 (MedChemExpress, USA, purity: 99.96%, C15H22N2O2) was utilized at a concentration of 1μM. Cell viability was assessed using the Cell Counting Kit-8 (Sigma, USA) following the provided instructions. ML385 (10μM, MedChemExpress, USA) was employed to inhibit Nrf2. Furthermore, Z-VAD-FMK (10μM, MedChemExpress, USA) and Necrosulfonamide (1 μM, MedChemExpress, USA) were also utilized.

Assay of intracellular reactive oxygen species (ROS)

ROS levels were measured using a ROS detection kit, specifically the highly sensitive DCFH-DA assay kit (Do Jindo, Japan). After removing the culture medium, cells in each group were washed twice with HBSS. Subsequently, the cells were treated with the DCFH-DA and DAPI working solution and incubated at 37℃ with 5% CO2 for 30 min in an incubator. Following removal of the working solution, additional washing with HBSS was performed. The examination involved the use of a sophisticated fluorescence microscope (DMI3000B, Leica, Germany). Quantitative analysis of intracellular ROS was conducted using a flow cytometer (BD, USA) with three replicates for each group.

Experimental groups and animals

Adult male Sprague–Dawley (SD) rats (10–12 weeks of age) were obtained from Hebei Medical University and maintained under standard conditions at 25 °C with a 12 h light–dark cycle and access to food and water ad libitum. The mice selected for the study weighed between 250 and 300 g. 96 SD rats were randomly divided into 4 groups: SHAM surgery group, ICH group, ICH + EGCG group, and ICH + ferroptosis inhibitor Fer-1 group. All experimental procedures were performed in accordance with the guidelines of the Animal Experimentation Ethics Committee of the Second Hospital of Hebei Medical University and in compliance with the National Institutes of Health Principles for the Care and Use of Laboratory Animals.

Establishment of intracerebral hemorrhage SD rat model

Rats were induced with general anesthesia using 2% sodium pentobarbital (40 mg/kg) and immobilized in a prone position with a stereotactic frame (NEUROSTAR, Germany). ICH was induced by infusing collagenase IV (Sigma-Aldrich, St. Louis, MO) into the right striatum of the rats. Collagenase IV, dissolved in 1 μL of saline, was delivered at a rate of 0.2 μL/min to induce brain injury related to ICH. Rats in the sham group underwent a similar procedure but received a saline infusion instead. In the EGCG group, rats were injected with EGCG (10 mg/kg) into the peritoneal cavity 2 h after collagenase IV administration, followed by daily doses for 5 days. The Fer-1 group received daily peritoneal injections of Fer-1 (2.5 μmol/kg, MCE, USA) for 5 days post-surgery, following a similar regimen to the EGCG group. After 5 days post-surgery, the SD rats were euthanized, and cerebral tissue samples were collected. Euthanasia uses carbon dioxide inhalation. SD rats are placed in a carbon dioxide anesthesia box. Carbon dioxide will enter the alveoli from the environment and then enter the brain through the blood. When the carbon dioxide content in the brain reaches a certain concentration, it will cause loss of consciousness and then death.

Neurological deficit scores and behavioral tests

The assessment of neurological deficits following intracerebral hemorrhage (ICH) involved using the modified Longa score and Bederson score on days 1, 3, and 5 post-model establishment. The Longa score, which ranges from 0 to 4, classifies: 0 as no neurological deficits, 1 as incomplete extension of the left forelimb, 2 as leftward rotation, 3 as leftward tilting, and 4 as lack of spontaneous walking and decreased consciousness levels. SD rats that scored 0 on the Longa scale did not show any neurological impairments, while those scoring 4 exhibited severe brain injury and were therefore excluded from the analysis. On the other hand, the Bederson score, which ranges from 0 to 5, represents: 0 for no deficits, 1 for forelimb flexion, 2 for forelimb flexion with reduced contralateral resistance, 3 for rotation towards the paralyzed side during free movement, 4 for rotary motion or associated seizures, and 5 for complete immobility. Higher Bederson scores indicate a greater extent of observed damage.

The sensory-motor functions were assessed using the Forelimb Placing Test (FPT) and Corner Turn Test (CTT). In the FPT, the forelimbs of the rats were allowed to freely extend. Independent evaluations were made by gently touching the corresponding whiskers to the edge of the table. Uninjured rats would quickly place their forelimbs on the tabletop and align them with the stimulated whisker. Depending on the extent of injury, the rats might place the contra-lateral forelimb on the stimulated whisker. Each forelimb underwent 10 trials, and the proportion of appropriate responses to whisker stimulation was determined. In the CTT, the rats were allowed to enter a corner at a 30° angle. The animals could then choose to turn left or right to exit the corner. The direction chosen by the rat was recorded for six repetitions, and the ratio of right turns was calculated.

Brain water content evaluation

On the fifth day post-creation of the ICH model in SD rats, the rats were anesthetized with 2% sodium pentobarbital at a dose of 40 mg/kg. Brain tissue was collected and divided into three parts: the left hemisphere, right hemisphere, and cerebellum. The brain samples were promptly weighed using an electronic balance (SARTORIUS, BS210S, Germany) to determine the wet weight (WW). Subsequently, the brain samples were dried at 100 °C for 24 h to determine the dry weight (DW). Brain water content was then calculated using the formula (WW - DW) / WW × 100%.

Analysis hematoma assessment

Five days after model induction, SD rats were sacrificed to evaluate the progression of hematoma. One rat was randomly selected from each group for immediate brain removal, followed by processing with 4% paraformaldehyde (PFA) from Solarbio in Beijing, China. The brain was then sliced into 1 mm sections, imaged using an Olympus stereomicroscope (SZX7), and the hematoma level in each section was recorded.

Paraffin section of rat brain

In order to preserve the brain tissue, rats were subjected to cardiac perfusion and treated with a 4% formaldehyde solution. The brain tissue was quickly collected and then immersed in a 4% paraformaldehyde solution at 4 °C for 6 h. Subsequently, paraffin embedding was performed, and the brain tissue embedded in paraffin was sliced into 5 μm thick sections and allowed to dry overnight at 60 °C.

Hematoxylin and eosin (HE) staining

Rat brain tissue from each experimental group was processed into paraffin sections at 60 °C for one hour. Deparaffinization was then performed twice using xylene, followed by rehydration through a sequential decrease in ethanol concentrations and distilled water. Subsequent steps included hematoxylin staining for 5 min, water rinsing for 15 min, and eosin staining for 30 s. Following rinsing with distilled water, dehydration was achieved through an ethanol gradient and xylene cleaning. Finally, the sections were sealed with a neutral mounting medium before observation and imaging using an optical microscope (DM200, Leica, Germany) were conducted.

Transmission electron microscope

On the fifth day following ICH induction, the impact of EGCG and Fer-1 on the mitochondrial structure in rats was investigated. The morphology of mitochondria was observed through transmission electron microscopy (HITACHI, Japan).

Fluoro-Jade C (FJC) staining

Neuronal staining of the repaired injury was performed using the FJC staining kit (TR-100-FJ, Biosensis, Australia). Paraffin-embedded sections were deparaffinized with xylene and then hydrated with ethanol. Following rinsing with distilled water, the sections were exposed to potassium permanganate for 15 min. Subsequently, they were treated with the FJC solution and co-incubated with DAPI solution. DPX was used as the mounting medium. The FJC-positive neurons were visualized using an inverted fluorescence microscope (DMI3000B, Leica, Germany). Each brain sample underwent three independent counts, and quantitative analysis was performed using Image J software (Image J 1.4, NIH, USA). The data were presented as the average number of FJC-positive neurons per square millimeter.

Evaluation of ferroptosis

Ferroptosis was evaluated by measuring iron content, malondialdehyde (MDA), and glutathione (GSH) levels in the brain tissue surrounding the hematoma in rats, as well as in primary cortical neurons. Approximately 1×10^6 rat primary cortical neurons from each group and 10 mg of brain tissue adjacent to the hematoma, collected following fresh pre-cooled PBS perfusion, were utilized for subsequent analyses. The levels of iron, MDA, and GSH in the brain tissue or primary cortical neurons surrounding the hematoma were quantified using the Iron Assay Kit (AB83366, ABCAM, USA), the Lipid Peroxidation Assay Kit (AB118970, ABCAM, USA), and the GSH Assay Kit (Nanjing Jianjie, China).

Cytotoxicity assay

The CCK-8 (Cell Counting Kit-8) assay kit (ZOMANBIO, ZP328, Beijing, China) was utilized to perform a CCK-8 experiment to evaluate cell proliferation or inhibition rates. Cells were grown in a 96-well plate and subjected to treatments according to group allocations. The control group functioned as the reference group for comparison purposes. Following treatment, a 10% CCK-8 solution was introduced to the culture medium and incubated for 2 h. Subsequently, the absorbance at 450 nm was measured to determine the cell viability in each group.

TUNEL staining

To quantitatively assess neuronal apoptosis, a dual staining protocol was carried out using the in situ apoptosis detection kit from Roche (Indianapolis, USA). This method involved staining NeuN (green) and TUNEL (red) in brain tissue sections collected 24 h post ICH, following the manufacturer's instructions. TUNEL-positive neurons were manually counted on six slices in the peri-hematoma region of each brain at 200x magnification. Quantification was performed using Image J software (version 1.4, NIH), and the results are reported as the percentage of TUNEL-positive neurons.

Flow cytometry analysis

Cell apoptosis was assessed through flow cytometry using Annexin V/PI double staining. Cells were stained with Annexin V-FITC (0.5 μg/mL) and PI (50 μg/mL) in the dark for 5 min, followed by analysis using FACSscan flow cytometry. The apoptotic rate was calculated by combining the percentages of early apoptosis (lower right quadrant) and late apoptosis (upper right quadrant) cells, and comparing this ratio between the hydroxybutyl vinyl ether-treated test group and the control group. FlowJo V10 software from Tree Star, Inc. was utilized for the analysis of cell cycle and apoptosis data.

RT-PCR

RNA extraction was conducted using the RNA extraction kit from Takara (Dalian, China), followed by quantification of RNA concentration. Subsequently, RNA was reverse transcribed into cDNA using the Prime Script RT kit from Takara. The generated cDNA was then used as a template for RT-PCR following the instructions of the SYBR R Premix Ex Taq II kit from Takara. The housekeeping gene GAPDH was employed as an internal control for calculating relative gene expression levels using the -ΔΔCt method.

Western blot

We extracted protein from the tissue around the hematoma. The Minute TM nuclear and cytoplasmic extraction kit (SC-003, Invent, USA) was used to separate the cell nucleus and cytoplasm. RIPA lysis buffer (Beyotime, China) was applied for lysing brain tissue and Primary cortical neuron. Protein concentration was determined using the BCA assay kit (23225, Thermo Fisher Scientific, USA). The homogenized protein samples were then separated by SDS-PAGE and transferred onto PVDF membranes (Sigma-Aldrich, USA). Following membrane blocking with 5% skim milk for 2 h, incubation overnight at 4 °C with primary antibodies was carried out: XCT (1:1000, AB175186, Abcam, USA), GPX4 (1:1000, AB125066, Abcam, USA), GAPDH (1:10000, ab181602, Abcam, USA), Histone H3 (1:1000, ab1791, Abcam, USA), Keap1 (1:1000, AF6261, Affinity Bioscience, China), P62 (1:1000, AF0016, Affinity Bioscience, China), Nrf2 (1:1000, ab92946, Abcam, USA). Subsequent incubation with a secondary antibody, rabbit anti-goat IgG(H&L)-DyLightTM 800 conjugated antibody (1:1000, ROCKL AND, USA) for 1 h followed. Visualization analysis was performed using the Odyssey Imaging System (Li-COR, USA), and band density was calculated using Image J software (1.4, NIH, USA).

Immunofluorescence

Frozen section of brain tissue around hematoma was selected. The primary antibodies employed included NEUN (1:200) (Abcam, ab7260, China), GPX4 (1:200, AB125066, Abcam, USA), and XCT (1:200, AB175186, Abcam, USA). Following overnight incubation with the primary antibodies, samples were subsequently treated with A488 IgG (1:500) (Abcam, ab182931, China) or A594 IgG (1:500) (Abcam, ab150116, China) secondary

antibodies for 2 h at room temperature the following day. DAPI was used to stain the nuclei. Images of the cell samples were captured using a fluorescence microscope (Leica DMi8, Germany).

Statistical analysis

GraphPad Prism 7 was used to conduct data analysis and create graphs. The summary data is presented as mean ± SEM. Neurological scores were analyzed using the Kruskal-Wallis test, followed by Dunn's multiple comparison test. The rest of the values were evaluated with a one-way ANOVA, followed by Tukey's multiple comparison test. Statistical significance was defined as $p < 0.05$.

Results

Incubation in vitro and identification of neurons

In order to investigate the mechanisms of neuronal cell death and identify potential targets for prevention and treatment of intracerebral hemorrhage, an in vitro culture of neurons from the rat cortex was established. By 4 h, the neurons adhered to the culture flask bottom, displaying a round shape with distinct refractivity, halo formation, and occasional cellular processes. Over the course of 24 h, there was a significant increase in the number of cellular processes and branches. By day 7, a highly interconnected cell network had formed. By day 14, some cellular processes exhibited slight retraction. As the culture time advanced, cell growth gradually slowed down, leading to cellular shrinkage, aging, and eventual cell death. The average survival time of cultured cells was approximately three weeks (Fig. 1A). Immunofluorescent staining of primary neuronal cells cultured for 14 days revealed positive expression of MAP2 and NSE, indicating their neuronal nature (Fig. 1B). Consequently, these in vitro cultured cells are suitable for further experiments and research. Four separate experiments were conducted for subsequent cell studies.

EGCG has a protective effect on Hemin induced ferroptosis and apoptosis of cortical neurons

Hemin was chosen as an in vitro model to mimic intracerebral hemorrhage, and the CCK8 assay was utilized to determine the appropriate concentration of Hemin for establishing the in vitro model. The results indicated that Hemin reduced the cell viability of primary cortical neurons, and a concentration resulting in approximately 50% cell viability was selected for inducing intracerebral hemorrhage (Fig. 1C). Subsequent investigations focused on the impact of EGCG on Hemin-induced cytotoxicity in primary cortical neurons. The CCK8 assay results revealed that EGCG enhanced cell viability in a concentration-dependent manner, similar to the iron death-selective inhibitor FER-1 (Fig. 1D). Erastin and RSL3, known inducers of ferroptosis, act as inhibitors of the cellular cystine/glutamate antiporter system Xc^- and GPX4. Our research demonstrated that EGCG could mitigate cell death induced by Erastin and RSL3 in the in vitro model of Hemin-induced neuronal injury, akin to the effect of FER-1 (Fig. 1E and F). Additionally, Hemin-induced depletion of GPX4 resulted in increased expression of the protective regulatory factor XCT transporter. Notably, EGCG treatment effectively boosted the expression of XCT and GPX4 (Fig. 1G, H and I). These findings indicate that EGCG (10μM) significantly upregulated the expression of XCT and GPX4. Based on the CCK8 assay results, EGCG (10μM) notably improved cell viability in the presence of Hemin, leading to its selection for subsequent in vitro experiments.

EGCG reduces the production of intracellular ROS

Intracellular ROS levels were measured by flow cytometry. Higher intensity correlated with higher ROS levels. Hemin group showed significantly higher fluorescence intensity compared to the control group. Conversely, EGCG (10μM) group displayed a notable decrease in fluorescence intensity, similar to the FER-1 group (Fig. 2A and B). This suggests that EGCG (10μM) partially mitigated the elevated intracellular ROS levels induced by Hemin. The reduction in intracellular ROS production highlights the potential of EGCG in inhibiting cellular oxidative stress and ferroptosis.

EGCG inhibits Hemin induced cell apoptosis

To explore the potential of EGCG in inhibiting Hemin induced apoptosis in primary cortical neurons, FACS analysis were conducted with 20μM Hemin in combination with either 10μM EGCG or 20 μM Fer-1. The results showed that treatment with EGCG or Fer-1 led to a decrease in the percentage of apoptosis triggered by Hemin (Fig. 2C and D).

EGCG reduces the production of MDA and Fe [2+] and reverses the downregulation of GSH, XCT, and GPX4

Hemin induced cortical neuronal cells exhibited significant signs of ferroptosis, including increased levels of intracellular MDA and Fe^{2+}, as well as depletion of GSH, XCT, and GPX4. Both EGCG (10μM) and FER-1 effectively reduced the elevated levels of intracellular MDA, Fe^{2+}, and GSH induced by Hemin (Fig. 2E, F and G). Furthermore, EGCG (10μM) or FER-1 significantly upregulated the expression of GPX4 (Fig. 2H and I) and XCT (Fig. 3A and C) in cortical neurons. JC-1 staining showed that EGCG or Fer-1 treatment resulted in a decreased percentage of Hemin induced early apoptosis (Fig. 3B and D). These observations indicate that EGCG has the ability to inhibit ferroptosis.

EGCG alleviates collagenase induced brain injury in rats

Brain imaging scans were used to assess the effectiveness of EGCG in reducing hematoma volume. Figure 4A illustrates significant brain tissue hematoma in the ICH group. Both the EGCG and FER-1 groups exhibited a notable reduction in hematoma volume post-ICH injury. Histological analysis with HE staining and Masson's staining indicated marked edema and necrosis in the brain tissue surrounding the hematoma in the ICH group (Fig. 4B and C), characterized by irregular cell arrangement, increased interstitial space, and infiltration

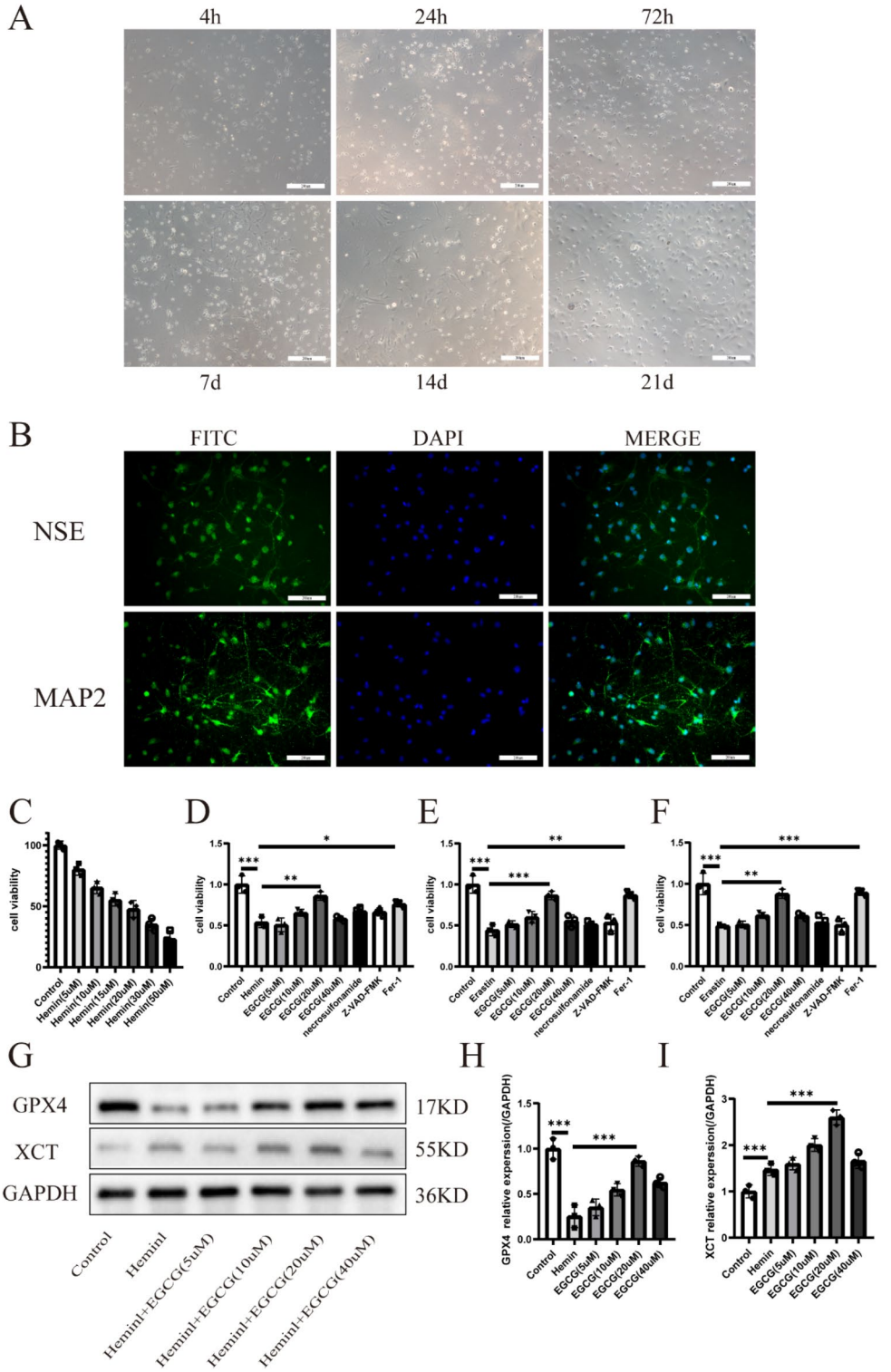

Fig. 1. EGCG can protect the cell viability of primary cortical neurons during in vitro iron death process. (**A**) Morphological changes of primary cortical neurons were observed under an inverted phase contrast microscope. (**B**) Immunofluorescence method was used to identify primary cortical neurons. (**C**, **G**) CCK8 was used to detect cell viability, and appropriate concentration of Hemin was selected to construct an in vitro cerebral hemorrhage model ($n = 3$). (**D**–**F**) Primary cortical neurons treated with Hemin, Erastin or RSL3, with different concentrations of EGCG (5μM, 10μM, 20μM, 40μM), necrosulfonamide (1μM), Z-VAD-FMK (10μM), or Fer-1 (10μM) for 24 h, then cell viability was measured ($n = 3$). (**G**) Western blot was performed on GPX4, XCT. (**H**–**I**) Statistical analysis of GPX4, XCT was performed ($n = 3$). Scale bars: A, B 200 μm; Data were expressed as mean ± standard deviation. $^{*}p < 0.05$, $^{**}p < 0.01$, $^{***}p < 0.001$, $^{****}p < 0.0001$.

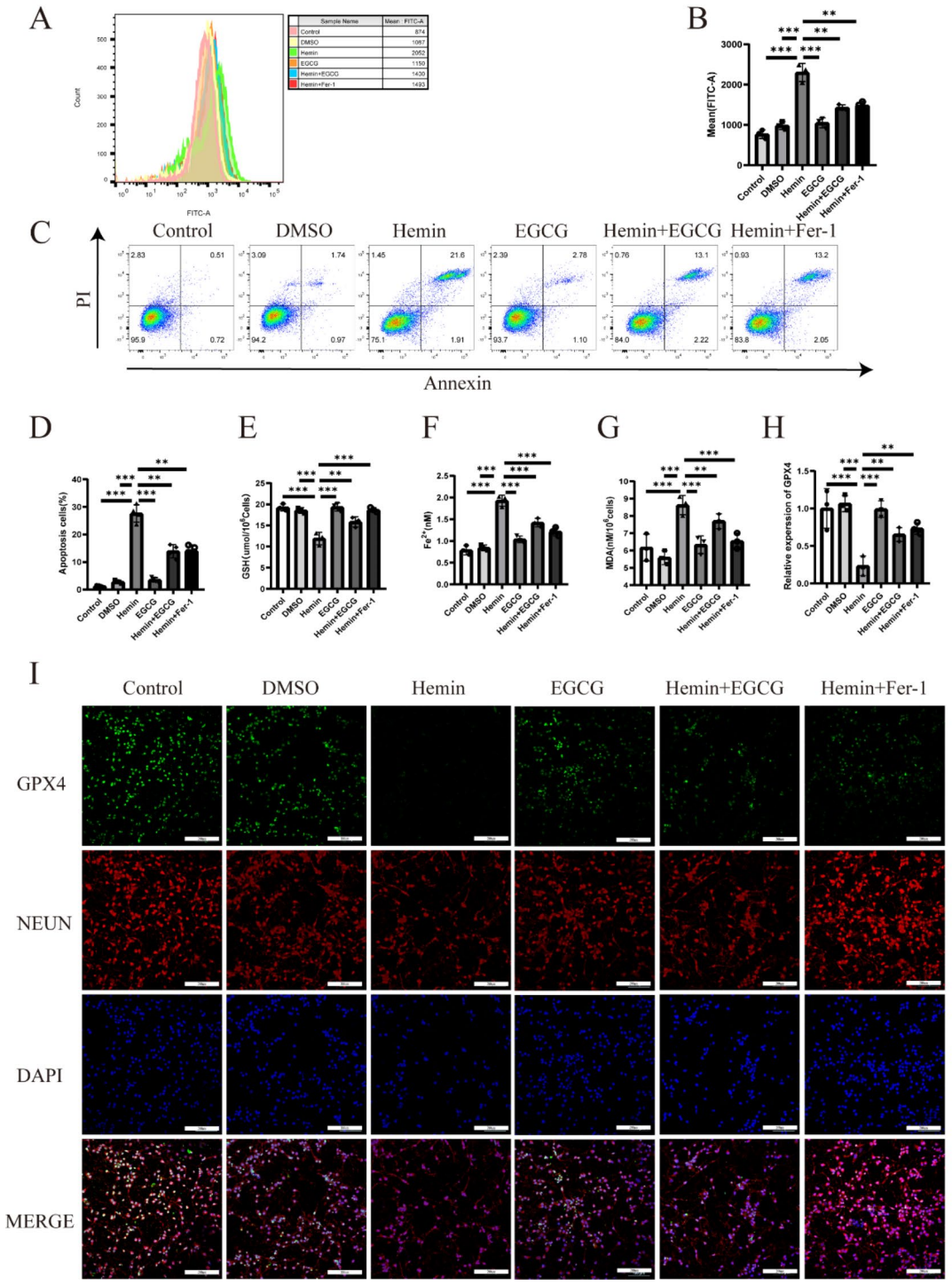

Fig. 2. The effects of EGCG on iron death and apoptosis of primary cortical neurons induced by Hemin. (**A** and **B**) Immunofluorescence probes were used to evaluate ROS levels by flow cytometry ($n=3$). (**C** and **D**) Evaluation of cellular apoptosis levels ($n=3$). (**E**, **F**, and **G**) Measurement of GSH levels, Fe2 + levels, and MDA levels in specified primary cortical neurons after 24 h of Hemin induction ($n=3$). (**H**) Statistical analysis of relative fluorescence intensity of GPX4 expression in different groups ($n=3$). (**I**) Expression analysis of GPX4 through immunofluorescent staining. Scale bars: I 200 μm; Data were expressed as mean ± standard deviation. $^{*}p<0.05$, $^{**}p<0.01$, $^{***}p<0.001$, $^{****}p<0.0001$.

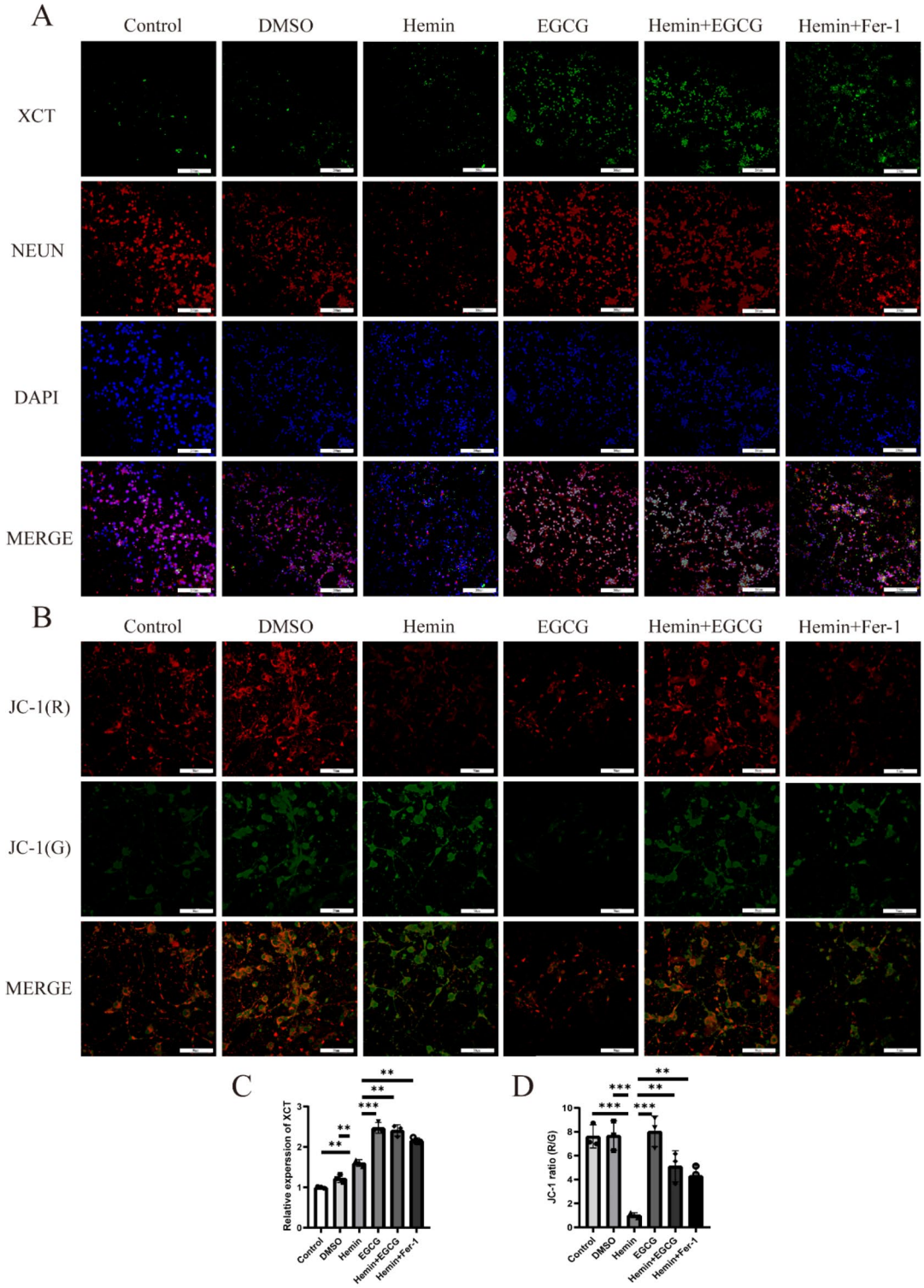

Fig. 3. The effects of EGCG on iron death and apoptosis of primary cortical neurons induced by Hemin. (**A** and **C**) Statistical analysis of relative fluorescence intensity of XCT expression in different groups ($n=3$). (**B** and **D**) Statistical analysis of relative fluorescence intensity of JC-1 expression in different groups ($n=3$). Scale bars: **A** 200 μm; **B** 50 μm. Data were expressed as mean ± standard deviation. $^{*}p<0.05$, $^{**}p<0.01$, $^{***}p<0.001$, $^{****}p<0.0001$.

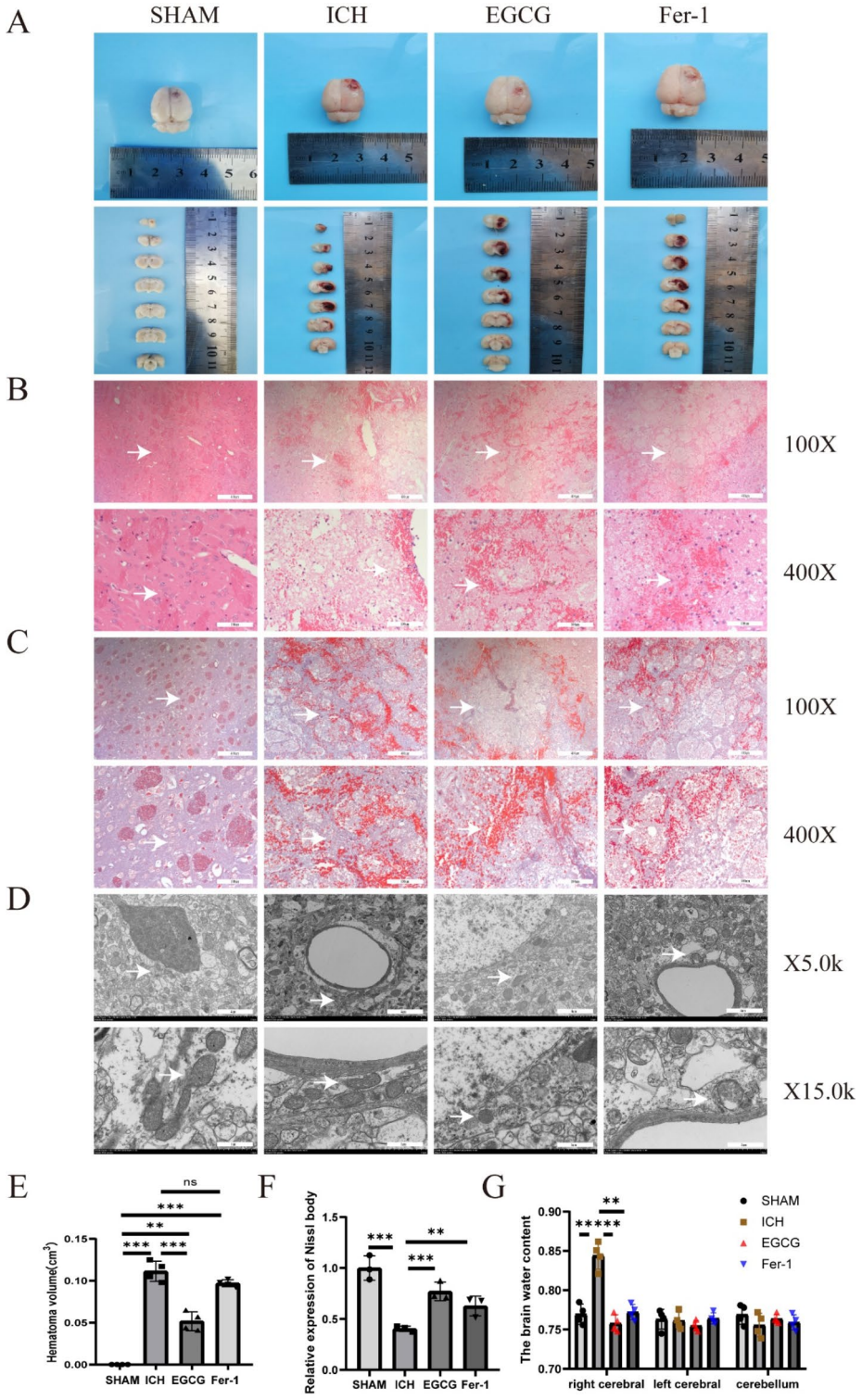

Fig. 4. EGCG alleviated brain damage caused by ICH in a collagenase rat model. (**A**–**C**) Representative images of hemorrhagic lesions, HE staining, and Cresyl Violet staining in rats from different groups. (**D**) Transmission electron microscopy was used to assess mitochondrial morphology in rats from different groups. (**E**) Volume quantification of hemorrhagic lesions ($n = 4$). (**F**) Nissl staining was performed to evaluate neuronal survival in rats from different groups ($n = 4$). (**G**) Brain water content was measured in each group to assess the effect of treatment on brain edema ($n = 12$). Scale bars: B, C 200/100μm; D 4/1μm. Data were expressed as mean ± standard deviation. $^{*}p < 0.05$, $^{**}p < 0.01$, $^{***}p < 0.001$, $^{****}p < 0.0001$.

of inflammatory cells. Conversely, the EGCG and FER-1 groups showed significantly attenuated pathological damage compared to the ICH group. Given the potential for cerebral hemorrhage-induced ferroptosis, transmission electron microscopy studies demonstrated that EGCG and FER-1 offered substantial protection against ICH induced brain tissue damage, preventing mitochondrial crest loss and outer membrane rupture (Fig. 4D). On the fifth day post-ICH, changes in Nissl bodies and brain water content were evaluated in various brain anatomical structures to assess treatment effects on brain edema. The results indicated an increase in Nissl bodies in the EGCG and FER-1 groups compared to the ICH group (Fig. 4E and F), along with a significant decrease in brain water content (Fig. 4G).

EGCG mitigates neurological functional deficits in rats after ICH

Neurobehavioral experiments were conducted on days 1, 3, and 5 following ICH surgery to evaluate the impact of EGCG and FER-1 on neurofunctional deficits. Neurological scores were assessed using the Longa and Bederson scales, while the FPT and CTT were utilized to evaluate motor and sensory function. In comparison to the SHAM group, the ICH group displayed a notable decrease in neurological scores 24 h post-surgery, which was significantly ameliorated with EGCG and FER-1 treatments (Fig. 5A and B). Moreover, both EGCG and FER-1 notably enhanced forelimb placement in ICH rats (Fig. 5C) and demonstrated improved performance in the CTT (Fig. 5D).

EGCG reduces neurodegeneration and iron-induced cell death in the perihematomal tissue of the brain

FJC staining was utilized to detect neuronal degenerative changes in dendrites, axons, and terminals. The findings revealed significant neuronal degeneration in the rat brain tissue surrounding the hematoma due to ICH injury. Treatment with EGCG and FER-1 notably reduced the number of FJC-positive cells compared to the ICH group, indicating the effectiveness of EGCG in mitigating iron deposition in the tissue surrounding the cerebral hemorrhage (Fig. 5E and F). To assess the impact of EGCG on ferroptosis in the rat ICH model, levels of MDA, GSH, and Fe^{2+} were measured. Cerebral hemorrhage rats exhibited elevated MDA levels, increased Fe^{2+} concentration, and decreased GSH levels. Treatment with EGCG and FER-1 led to significant improvements in MDA, GSH, and Fe^{2+} levels compared to the ICH group (Fig. 5G and I). TUNEL staining demonstrated that EGCG and FER-1 treatment significantly ameliorated collagenase-induced brain injury in rats compared to the ICH group (Fig. 6A and C).

EGCG reduces iron death and apoptosis in rats with cerebral hemorrhage through Keap1/P62/Nrf2 pathway

Given the importance of Nrf2 in ferroptosis and apoptosis regulation, along with key downstream proteins GPX4, XCT, BAX, BCL-2, and CASP3, our study aimed to explore the potential of EGCG in enhancing Nrf2 activity through the Keap1/P62/Nrf2 pathway. Utilizing network pharmacology analysis, we identified Keap1 as a target gene for EGCG, a known upstream regulator of Nrf2. Western blotting was employed to evaluate protein phosphorylation levels and relevant protein expression. Compared with ICH group, EGCG group significantly increased Keap1 and P62 expression, enhanced Nrf2 nuclear translocation, increased XCT, GPX4 and BCL-2 levels, and decreased BAX and CASP3 levels (Fig. 6B and L).

EGCG significantly reduces hemin induced ferroptosis and apoptosis in primary cortical neurons through the Keap1/P62/Nrf2 pathway

Treatment with EGCG activated Keap1 and P62, promoting the nuclear translocation of Nrf2 in primary cortical neurons, leading to subsequent changes in ferroptosis and apoptosis (Fig. 7). In contrast, FER-1 showed a weaker ability. Further investigations were carried out to examine the activation of Keap1 and P62 mediated by EGCG and the nuclear translocation of Nrf2 in primary cortical neurons treated with EGCG in the presence or absence of K67 and ML385. K67 inhibited the activation of Keap1 and P62, nuclear expression of Nrf2, as well as the expression levels of XCT, GPX4, BAX, BCL-2, and CASP3 induced by EGCG. However, ML385 inhibited the nuclear expression of Nrf2, expression levels of XCT, GPX4, BAX, BCL-2, and CASP3, but did not significantly affect the activation of Keap1 and P62 (Fig. 8). The results in Fig. 9 suggest that EGCG plays a regulatory role in ferroptosis and apoptosis through the induction of Keap1 and P62 activation and nuclear translocation of Nrf2.

Discussion

ICH is a highly lethal subtype of hemorrhagic stroke with a high mortality rate within one month after onset[26]. The primary injury is caused by physical damage from blood extravasation, increased intracranial pressure, and surrounding edema[27], while the secondary injury is triggered by peripheral vascular neurotoxicity and cell death induced by hemoglobin, heme, and iron. Despite advancements in minimally invasive surgical treatments for ICH, specific therapeutic tools remain scarce. Understanding the disease's pathophysiology is essential for developing new diagnostic and therapeutic approaches. Recent research indicates that hemoglobin/heme/iron significantly contribute to delayed brain edema and irreversible neuronal damage post-ICH[28]. Iron release from hemoglobin post-ICH leads to the generation of ROS, causing oxidative stress and secondary brain injury in neural cells[29]. Heme induces lipid peroxidation and the production of various reactive oxygen species, resulting in cellular harm. There is growing evidence suggesting that ferroptosis may play a crucial role in this process, making it a promising target for future ICH therapy.

Ferroptosis is a form of cell death that relies on the control of iron ions, resulting in the generation of elevated levels of reactive oxygen species[30]. The distinct alterations linked with ferroptosis are instigated by the substantial accumulation of detrimental reactive oxygen species and lipid peroxides stemming from the Fenton reaction. The excess iron accumulation supplies an abundance of ferrous ions for the Fenton reaction, leading to

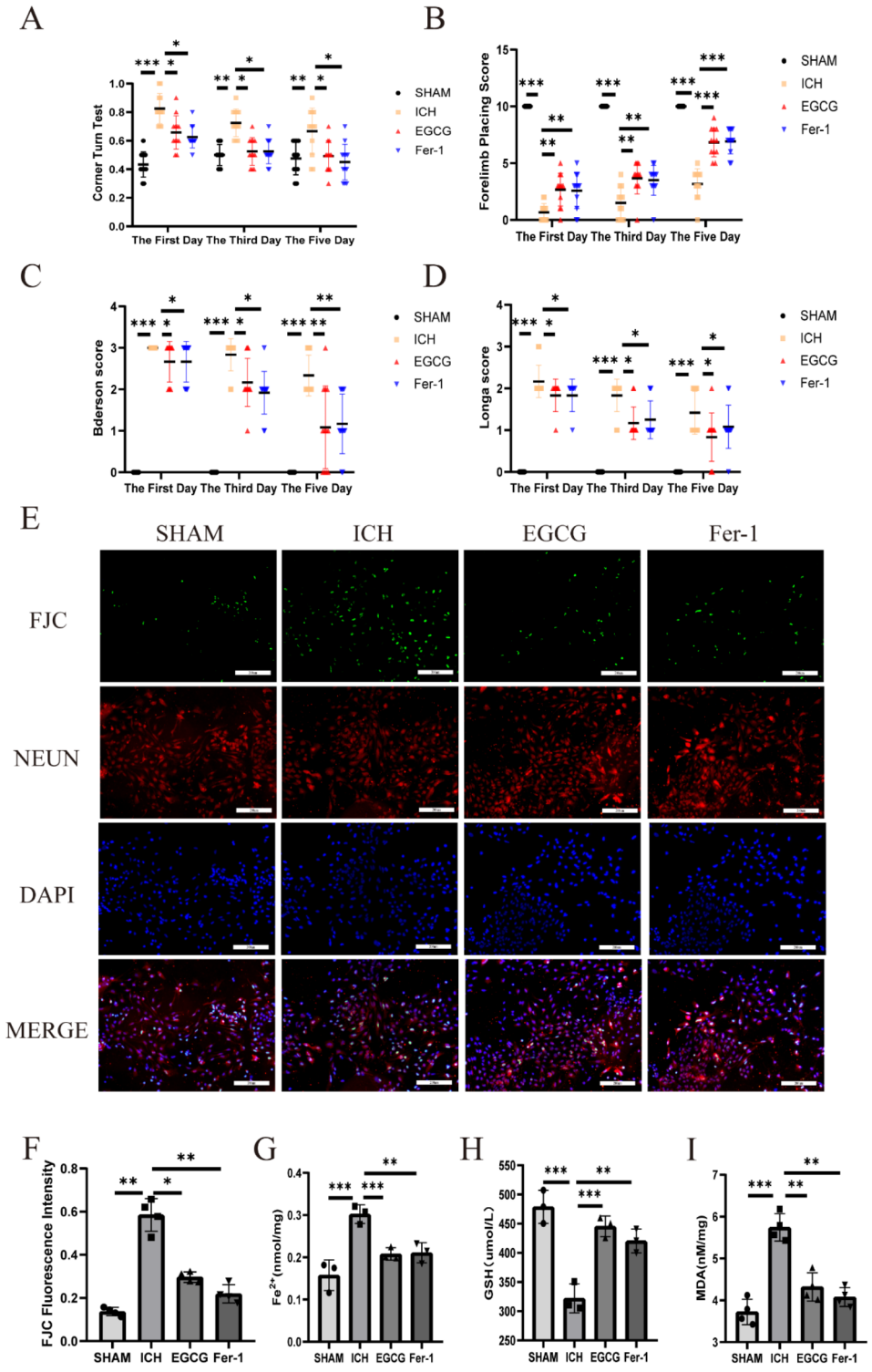

Fig. 5. EGCG alleviated brain damage caused by ICH in a collagenase rat model. (**A**) Corner turn test conducted from day 1 to day 5 after ICH ($n=12$). (**B**) Forelimb placement test ($n=12$). (**C**) Longa score and (**D**) Pedersen score were used to evaluate neurological function recovery ($n=12$). (**E** and **F**) Representative images of Fluoro-Jade C (FJC) staining in brain sections of rats from different groups ($n=4$). (**G**, **H**, and **I**) Levels of Fe2+, GSH, and MDA in the brain tissue surrounding the intracerebral hemorrhage were evaluated on the 5th day after ICH ($n=4$). Scale bars: E 200 μm; D 4/1μm. Data were expressed as mean ± standard deviation. $^{*}p<0.05$, $^{**}p<0.01$, $^{***}p<0.001$, $^{****}p<0.0001$.

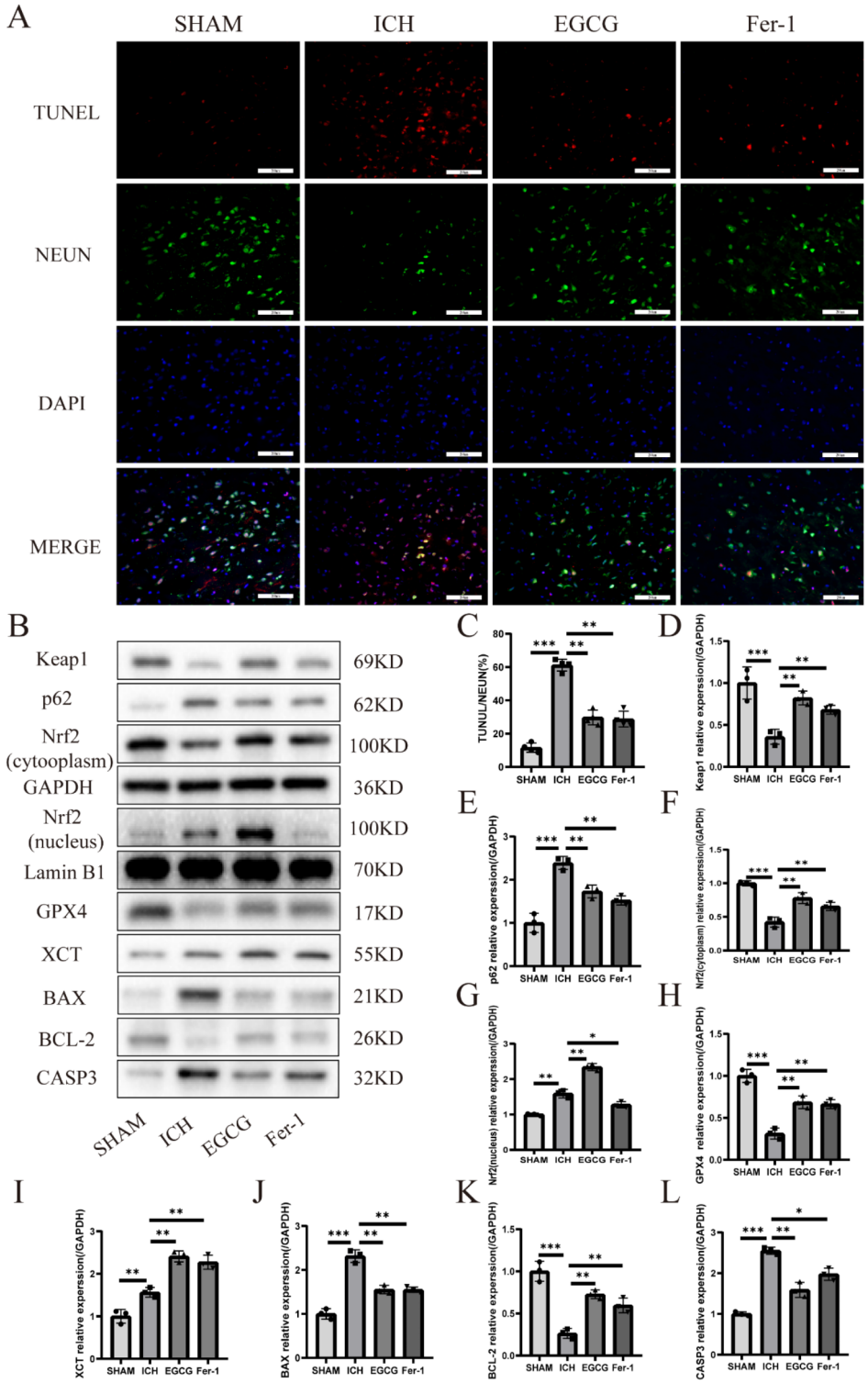

Fig. 6. EGCG treatment significantly reduces iron death and apoptosis in ICH rats through the Keap1/P62/Nrf2 pathway. (**A** and **C**) TUNEL staining was performed to detect cellular apoptosis in different groups ($n=4$). (**B**) Protein expression levels of Keap1, P62, Nrf2, GPX4, XCT, BAX, BCL-2, and CASP3 were analyzed using Western blot. (**D**–**L**) Protein expression levels in different groups were analyzed using Western blot ($n=4$). Scale bars: **A**200 μm. Data were expressed as mean ± standard deviation. $^{*}p<0.05$, $^{**}p<0.01$, $^{***}p<0.001$, $^{****}p<0.0001$.

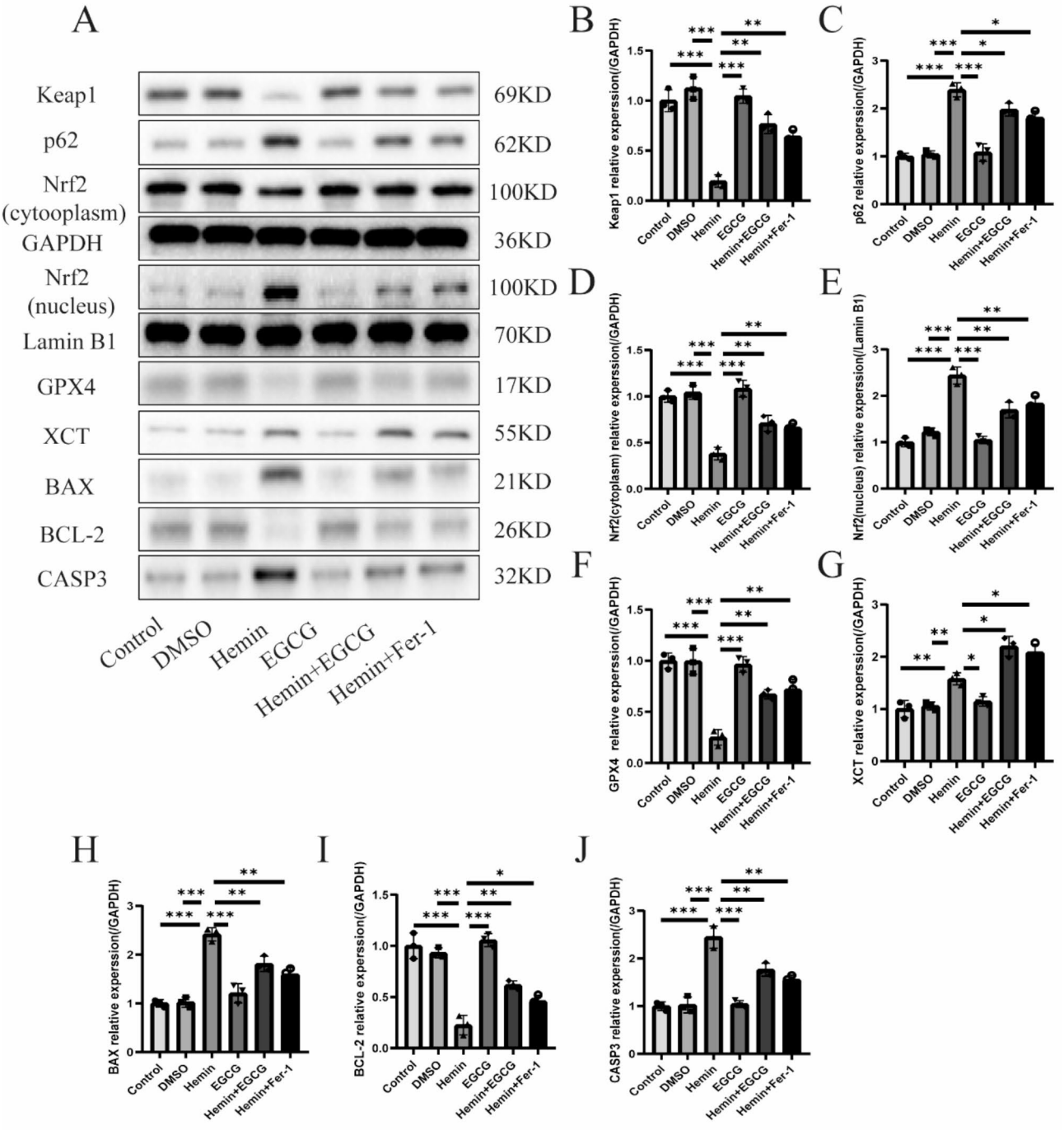

Fig. 7. EGCG treatment significantly reduces iron death and apoptosis in primary cortical neurons through the Keap1/P62/Nrf2 pathway. (**A**) Protein expression levels of Keap1, P62, Nrf2, GPX4, XCT, BAX, BCL-2, and CASP3 were analyzed using Western blot. (**B**–**J**) Protein expression levels in different groups were analyzed using Western blot ($n=3$). Data were expressed as mean ± standard deviation. $^{*}p<0.05$, $^{**}p<0.01$, $^{***}p<0.001$, $^{****}p<0.0001$.

an excessive production of hydroxyl and hydroxyl radical species. This heightened generation of reactive oxygen species induces harm to nucleic acids, proteins, and cell membranes, exacerbating the damage[31]. The significant rise in hemoglobin/heme/iron levels subsequent to intracerebral hemorrhage triggers ferroptosis. However, there is a scarcity of research on the categorization of neuronal cell death and the related regulatory mechanisms post-intracerebral hemorrhage, making further investigation into neuronal ferroptosis a current intricate and trending research domain. The identification of specific medications for the management of intracerebral hemorrhage is essential to tackle this challenge.

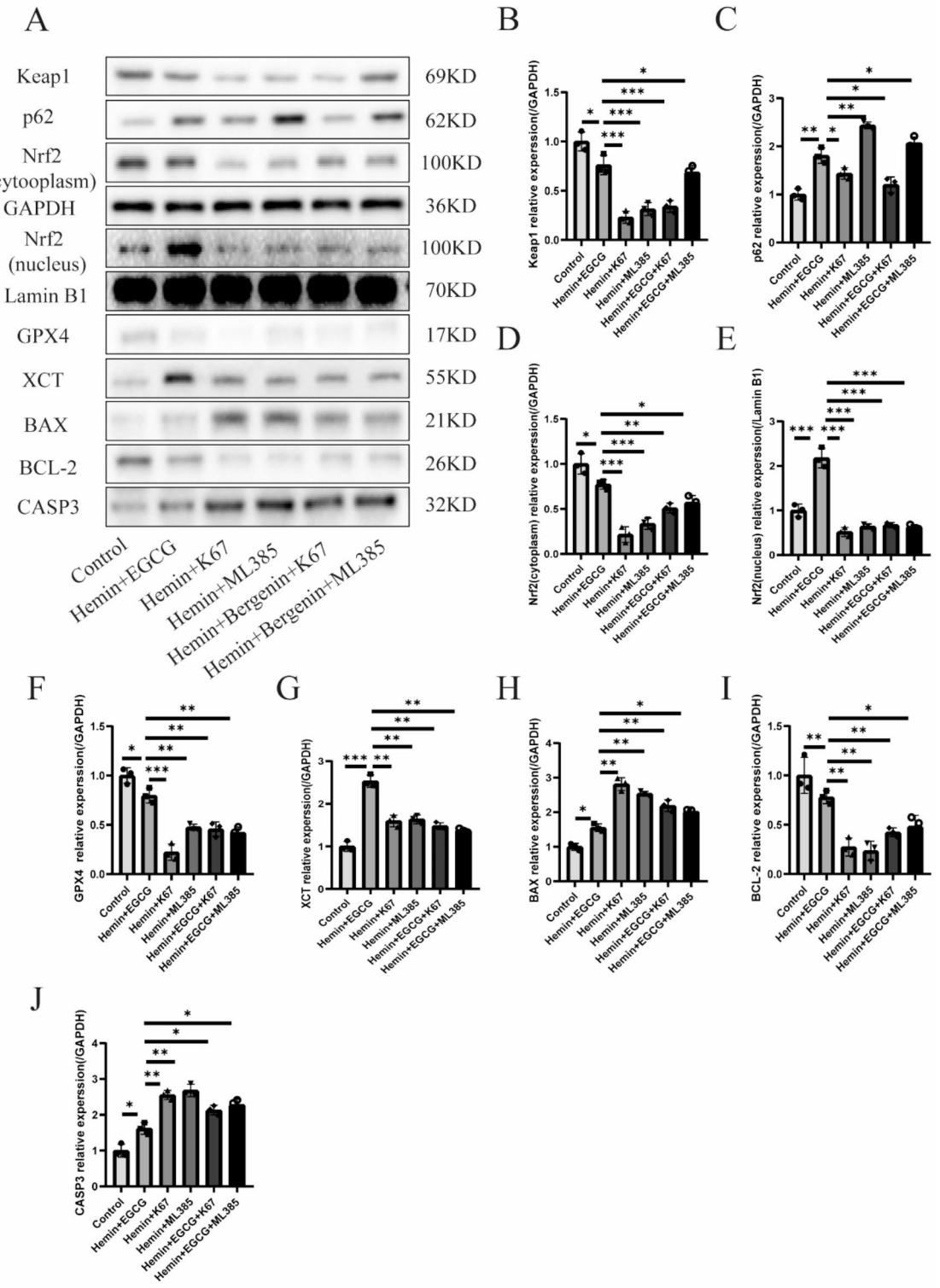

Fig. 8. EGCG treatment significantly reduces iron death and apoptosis in primary cortical neurons through the Keap1/P62/Nrf2 pathway. (**A**) Protein expression levels of Keap1, P62, Nrf2, GPX4, XCT, BAX, BCL-2, and CASP3 were analyzed using Western blot. (**B**–**J**) Protein expression levels in different groups were analyzed using Western blot ($n=3$). Data were expressed as mean ± standard deviation. $^{*}p<0.05$, $^{**}p<0.01$, $^{***}p<0.001$, $^{****}p<0.0001$.

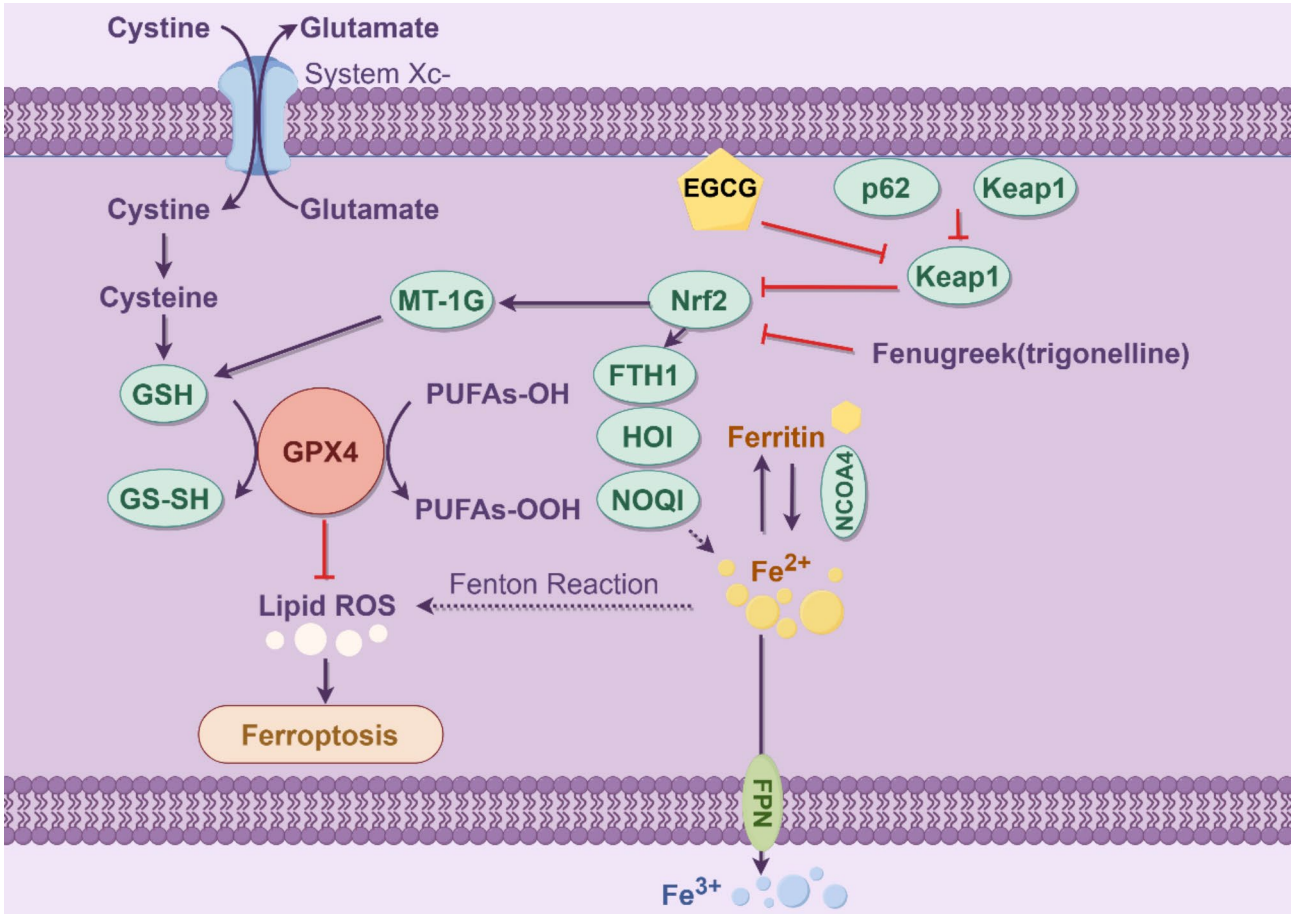

Fig. 9. EGCG treatment significantly reduces iron death and apoptosis in primary cortical neurons through the Keap1/P62/Nrf2 pathway.

Cell apoptosis, also known as programmed cell death, is a fundamental physiological process controlled by intricate signaling networks within the cell[32]. It plays a crucial role in preserving the health and equilibrium of organismal tissues by inducing key changes such as cell membrane budding, nuclear fragmentation, chromatin condensation, and disruption of intracellular structures. These alterations are orchestrated through the activation of apoptotic signaling pathways, which involve mitochondrial regulation, caspase protease family activation, and DNA fragmentation[33]. Cell apoptosis is indispensable for maintaining tissue homeostasis and normal development, facilitating the removal of excess or faulty cells during development to ensure proper tissue and organ formation and function. Furthermore, it contributes to physiological functions like immune response, tumor suppression, and clearance of infections. Nonetheless, aberrant regulation of cell apoptosis can result in diseases such as cancer and autoimmune disorders. Consequently, research on neuronal apoptosis following intracerebral hemorrhage has emerged as a current, intricate subject, necessitating the identification of specific drugs for treatment to enhance the situation.

EGCG, a naturally occurring compound from the catechin class of flavonoids, is predominantly found in tea, particularly green tea, in substantial quantities. It demonstrates a range of biological activities and pharmacological effects, including antioxidant, anti-inflammatory, anticancer, anti-aging, and cardioprotective properties. EGCG can scavenge free radicals, alleviate cellular oxidative stress, and protect cells from damage. In vitro experiments have shown that EGCG can enhance cell viability in primary cortical neurons induced by Hemin, as well as significantly improve cell viability when exposed to broad-spectrum ferroptosis inducers Erastin and RSL3. Previous studies have indicated that EGCG has the potential to inhibit the production of MDA and intracellular ROS induced by iron, suggesting its role as an iron chelator [26,27]. Furthermore, EGCG has been considered a promising therapeutic agent for iron-mediated ferroptosis associated with intracerebral hemorrhage. Recent research has also highlighted EGCG's efficacy in treating stroke and ischemia/reperfusion (I/R) injury, making it a valuable drug for cerebrovascular diseases[34]. Pharmacokinetic studies have demonstrated that EGCG can easily cross the blood-brain barrier, providing significant neuroprotective effects. Its metabolites exhibit high antioxidant activity[35–37]. Treatment with EGCG has been shown to impact brain tissue, reduce brain edema post-injury, improve neurofunctional deficits, and enhance anti-inflammatory and antioxidant capacities[29]. For in vivo experiments, previous studies have demonstrated that EGCG at a dose of 10 mg/kg can have a significant impact on damaged brain tissue, leading to notable improvements in neurofunctional deficits, brain hemorrhage, and disruption of the blood-brain barrier[38,39]. As a result, we decided to use this concentration for

our own in vivo experiments. In our subsequent experiments, rats were intraperitoneally injected with EGCG at a dose of 10 mg/kg 2 h after model establishment, once daily for six consecutive days. The rats that received EGCG exhibited significant enhancements in neurobehavioral tests, indicating a clear therapeutic effect.

EGCG has been demonstrated to effectively reduce iron accumulation in the brain tissue surrounding the hematoma and ameliorate neuronal degeneration resulting from cerebral hemorrhage, indicating its therapeutic promise in iron-induced neuronal ferroptosis post intracerebral hemorrhage. Studies suggest that agents inhibiting iron-induced ferroptosis can mitigate brain damage in animal models of cerebral hemorrhage, proposing these inhibitors as potential pharmaceuticals for treating cerebral hemorrhage[22]. Specifically, Fer-1, an inhibitor of iron-induced ferroptosis, has been shown to enhance neuroprotection and alleviate acute brain hemorrhage injury by mitigating iron-induced ferroptosis. This mechanism involves the suppression of ROS generation and reduction of iron accumulation to prevent neuronal demise[23]. Consequently, Fer-1 was employed as a positive control in subsequent experiments to investigate the potential regulatory mechanisms of EGCG in modulating iron-induced ferroptosis following cerebral hemorrhage.

Under normal conditions, the protein Nrf2 is typically found in the cytoplasm where it is inhibited by Keap1, preventing its movement into the nucleus. However, when oxidative stress occurs, Nrf2 separates from Keap1 and translocates into the nucleus to regulate the expression of antioxidant proteins such as HO-1 [40,41]. Previous studies have shown that ginsenoside Rk1 possesses anti-inflammatory and antioxidant properties by modulating the Keap1/P62/Nrf2 signaling pathway[42]. The current research demonstrated that treatment with Hemin decreased the levels of nuclear Nrf2 in primary cortical neurons, while treatment with EGCG promoted the translocation of Nrf2 into the nucleus. This led to an increase in the expression of GPX4, XCT, and BCL-2, as well as a decrease in the levels of BAX and CASP3. These results suggest that the activation of the Keap1/P62/Nrf2 pathway plays a role in the protective effects of EGCG against iron-induced ferroptosis and apoptosis in primary cortical neurons exposed to Hemin-induced damage. This mechanism aligns with previous findings on the anti-neuroinflammatory effects observed by activating the Nrf2/HO-1 pathway in microglial cells[43,44].

This study suggests that EGCG inhibits iron death and apoptosis induced by cerebral hemorrhage in rats by activating the Keap1/P62/Nrf-2 signaling pathway. These results propose a novel therapeutic strategy utilizing EGCG for the treatment of cerebral hemorrhage, highlighting the significance of these mechanisms. Furthermore, targeting Nrf2 activation via the Keap1/P62/Nrf-2 pathway shows promise as a potential treatment approach. While this research offers insights into cerebral hemorrhage treatment, further validation is required to confirm the experimental results and investigate clinical implications.

Conclusions

The results showed that EGCG enhanced the activation of the Keap1/P62/Nrf-2 signaling pathway, thereby inhibiting oxidative stress, iron death, and apoptosis in a rat cerebral hemorrhage model. This suggests that EGCG has a potential protective effect on neuronal damage in rats with cerebral hemorrhage, supporting its therapeutic application in neurological diseases.

Data availability

The data used to support the findings of this study are included in the article.

Received: 28 June 2024; Accepted: 10 December 2024
Published online: 28 December 2024

References

1. Cordonnier, C., Demchuk, A., Ziai, W., & Anderson, C.S. Intracerebral haemorrhage: Current approaches to acute management. *Lancet 2018 Oct 6* **392**(10154), 1257–1268
2. van Asch, C.J. et al. Incidence, case fatality, and functional outcome of intracerebral haemorrhage over time, according to age, sex, and ethnic origin: A systematic review and meta-analysis. *Lancet Neurol.* **9**(2), 167–176 (2010).
3. Gross, B. A., Jankowitz, B.T., & Friedlander, R. M. C. I. Hemorrhage: A Rev *JAMA* **321**(13):1295–1303. (2019).
4. Babadjouni, R. M., Radwanski, R.E., Walcott, B.P., et al. Neuroprotective strategies following intraparenchymal hemorrhage. *J. Neurointerv. Surg.* **9**(12), 1202–1207 (2017).
5. Chen, Y., Liu, Z., & Gong, Y. Neuron-immunity communication:mechanism of neuroprotective effects in EGCG. *Crit. Rev. Food Sci. Nutr.* **22**:1–20 .
6. Yu, Q. et al. EGCG attenuated acute myocardial infarction by inhibiting ferroptosis via miR-450b-5p/ACSL4 axis. *Phytomedicine* **119**, 154999 (2023).
7. Wang, J., Zhu, B., & Tang, Y. EGCG modulates PKD1 and ferroptosis to promote recovery in ST rats. *Transl. Neurosci.* **11**(1), 173–181 (2020).
8. Xie, L. W., Cai, S., Zhao, T.S., Li, M., & Tian, Y. Green tea derivative (-)-epigallocatechin-3-gallate (EGCG) confers protection against ionizing radiation-induced intestinal epithelial cell death both in vitro and in vivo. *Free Radic. Biol. Med.* **161**, 175–186 (2020).
9. Xia, Y., Wang, H., Xie, Z., Liu, Z.H., & Wang, H. L. Inhibition of ferroptosis underlies EGCG mediated protection against Parkinson's disease in a Drosophila model. *Free Radic. Biol. Med.* **211**, 63–76 (2024).
10. Huang, L., Wang, X., Zheng, Y. & Chen, Y. EGCG-NPs inhibition HO-1-mediated reprogram iron metabolism against ferroptosis after subarachnoid hemorrhage. *Redox Biol.* **70**, 103075 (2024).
11. Li, F., Hao, S. Gao, J., & Jiang, P. EGCG alleviates obesity-exacerbated lung cancer progression by STAT1/SLC7A11 pathway and gut microbiota. *J. Nutr. Biochem.* **120**, 109416 (2023).
12. Stepanić, V. & Kučerová-Chlupáčová, M.R. Chemoinformatic analysis of ferroptosis modulators with a focus on. *Nat. Plant. Prod. Mol.* **28**(2), 475 (2023).
13. Yang, C., Chen, D., Tang, Q et al. Epigallocatechin-3-Gallate alleviates liver oxidative damage caused by Iron overload in mice through. *Inhibi. Ferroptosis Nutr.* **15**(8), 1993 (2023).
14. Yu, H., Song, Z., Yu, J. & Ren B. Supramolecular self-assembly of EGCG-selenomethionine nanodrug for treating osteoarthritis. *Bioact. Mater.* **32**, 164–176 (2023).
15. Dixon, S. J. et al. Ferroptosis: An iron-dependent form of nonapoptotic. *Cell. Death Cell.* **149**(5), 1060–1072 (2012).

16. Li, D., & Li, Y.The interaction between ferroptosis and lipid metabolism in cancer. *Signal. Transduct. Target. Ther.* **5**(1), 108 (2020).
17. Mao, X. Y. Zhou, H.H., & Jin, W.L. Ferroptosis induction in Pentylenetetrazole Kindling and Pilocarpine-Induced epileptic seizures in mice. *Front. Neurosci.* **13**, 721 (2019).
18. Wan, J., Ren, H., & Wang, J. Iron toxicity, lipid peroxidation and ferroptosis after intracerebral haemorrhage. *Stroke Vasc Neurol.* **4**(2), 93–95 (2019).
19. Stockwell, B. R. et al. Ferroptosis: A regulated cell death nexus linking metabolism, redox biology. *Disease Cell.* **171**(2), 273–285 (2017).
20. Salvador, G. A. Iron in neuronal function and dysfunction. *Biofactors* **36**(2):103 –10. (2010)
21. Skouta, R. et al. Ferrostatins inhibit oxidative lipid damage and cell death in diverse disease models. *J. Am. Chem. Soc.* **136**(12), 4551–4556 (2014).
22. Ma, S. et al. Evaluation of the anti-inflammatory activities of tanshinones isolated from Salvia Miltiorrhiza var.alba roots in THP-1 macrophages. *J. Ethnopharmacol.* **188**, 193–199 (2016).
23. Spatafora, C. Tringali, C. Natural-derived polyphenols as potential anticancer agents. *Anticancer Agents Med. Chem.* **12**, 902–918 (2012).
24. Su, C. Y. et al. Salvia miltiorrhiza: Traditional medicinal uses, chemistry, and pharmacology. *Chin. J. Nat. Med.* **13**, 163–182 (2015).
25. Zhang, W. et al. Salvianolic acid a attenuates ischemia reperfusion induced rat brain damage by protecting the blood brain barrier through MMP-9 inhibition and anti-inflammation. *Chin. J. Nat. Med.* **16**(3), 184–193 (2018).
26. Bao, B., Yin, X.P., Wen, X.Q., Suo, Y.J., Chen, Z.Y. Li, D.L.L.Q., Cao, X.M., & Qu, Q.M. The protective effects of EGCG was associated with HO-1 active and microglia pyroptosis inhibition in experimental intracerebral hemorrhage. *Neurochem Int.* **170**, 105603 (2023).
27. Sun, Y., Li, Q., Guo, H. & He, Q. F. Iron Metabolism after Intracerebral Hemorrhage Cells. **12**(1):90 (2022)
28. VanDuyse, S. A. Fulford, M.J., & Bartlett, M.G. ICH Q10 Pharmaceutical quality system guidance: Understanding its impact on pharmaceutical quality. *AAPS J.* **23**(6), 117 (2021).
29. Yang, W., GFeng, H., Hu, R. Exosomes from young healthy human plasma promote functional recovery from intracerebral hemorrhage via counteracting ferroptotic injury. *Bioact Mater.* **27**, 1–14 (2023).
30. Zhou, Z. X. et al. A inhibits ferroptosis and protects against intracerebral hemorrhage. *Neural Regen Res.* **18**(6), 1308–1315. https://doi.org/10.4103/1673-5374.355822.PMID:36453416;PMCID:PMC9838153 (2023).
31. Zhang, Y., Liu, Y. & Yong, V.W., Xue, M. Omarigliptin inhibits brain cell ferroptosis after intracerebral hemorrhage. *Sci. Rep.* **13**(1), 14339. https://doi.org/10.1038/s41598-023-41635 (2023)
32. Zhou, T. & Zhu, M. Liang Z. Epigallocatechin-3-gallate modulates peripheral immunity in the MPTP-induced mouse model of Parkinson's disease. *Mol. Med. Rep.* **17**, 4883–4888 (2018).
33. Cheng, C. Y. et al. Chin T.Y.,Hsieh M.F.Epigallocatechin-3-gallate-loaded liposomes favor anti-inflammation of microglia cells and promote neuroprotection. *Int. J. Mol. Sci.* **22**, 3037 (2021).
34. Wang, F., Han, Y., Xi, S. & Lu, Y. Catechins reduce inflammation in lipopolysaccharide-stimulated dental pulp cells by inhibiting activation of the NF-κB pathway. *Oral Dis.* **26**, 815–821. https://doi.org/10.1111/odi.13290 (2020).
35. Stephenson, J., Nutma, E., Van Der Valk, P., & Amor, S. Inflammation in CNS neurodegenerative diseases. *Immunology* **154**, 204–219 (2018).
36. Liu, S.F., & Malik, A.B. NF-kappa B activation as a pathological mechanism of septic shock and inflammation. *Am. J. Physiol. Lung Cell. Mol. Physiol.* **290**, L622–L645. https://doi.org/10.1152/ajplung.00477.2005 (2006).
37. Zhong, X., Wei B., & Wei, M. Epigallocatechin-3-Gallate attenuates microglial inflammation and neurotoxicity by suppressing the activation of Canonical and Noncanonical Inflammasome via TLR4/NF-κB pathway. *Mol. Nutr. Food Res.* **63**, e1801230 (2019).
38. Liu, T., Zhang, L., Joo, D. & Sun, S.C. NF-κB signaling in inflammation. *Signal. Transduct. Target. Ther.* **2**, 17023 https://doi.org/10.1038/sigtrans.2017.23 (2017).
39. Feng, C. et al. Disulfide suppresses the inflammation and apoptosis Resistance Induced by DCA through ROS and the NF-κB signaling pathway in Human Barrett's epithelial cells. *Inflammation* **40**, 818–831. https://doi.org/10.1007/s10753-017-0526-4 (2017).
40. Nam, N. H. Naturally occurring NF-kappaB inhibitors. *Mini Rev. Med. Chem.* **6**, 945–951 (2006).
41. Luqman, S. & Pezzuto, J. M. NFkappaB: A promising target for natural products in cancer chemoprevention. *Phytother Res.* **24**, 949–963. https://doi.org/10.1002/ptr.3171 (2010).
42. Walmsley, S. R., Sabroe I. et al. Prolyl hydroxylase 3 (PHD3) is essential for hypoxic regulation of neutrophilic inflammation in humans and mice. *J. Clin. Investig* **121**, 1053–1063. https://doi.org/10.1172/JCI43273 (2011).
43. Koshikawa, N., Hayashi, J., Nakagawara, A., & Takenaga, K. Reactive oxygen species-generating mitochondrial DNA mutation up-regulates hypoxia-inducible factor-1alpha gene transcription via phosphatidylinositol 3-kinase-Akt/protein kinase C/histone deacetylase pathway. *J. Biol. Chem.* **284**, 33185–33194 (2009).
44. Peng, X. et al. Attenuates Hypoxia-Induced inflammation in BV2 microglia by inhibiting oxidative stress and NF-κB/Hif-1α signaling. *BioMed. Res. Int.* **2020**, 8978704 https://doi.org/10.1155/2020/8978704 (2020).

Acknowledgements

Central Guiding Local Science and Technology Development Fund Projects (236Z7752G); the Medical Research Project of Hebei Provincial Health Commission (20230031); Special Project for the Construction of Hebei Province International Science and Technology Cooperation Base (193977143D).

Author contributions

Liang Hao and Aobo Zhang made the same contribution. Liang Hao, Aobo Zhang and Liqiang Liu designed the study and wrote the manuscript. Aobo Zhang, Dongsheng Lv, LuLu Cong, Zhimin Sun performed the behavioral testing and experiments and analyzed the data. Liang Hao, Aobo Zhang and Liqiang Liu contributed to revising the manuscript. All authors read and approved the final manuscript.

Competing interests

The authors declare no competing interests.

Ethics approval

The animal study was reviewed and approved by the Ethics Committee of The Second Hospital of Hebei Medical University. This study was conducted following the guidelines outlined in the ARRIVE (Animal Research: Reporting of In Vivo Experiments) guidelines. All methods in this study were conducted in accordance with the relevant guidelines and regulations" in the manuscript.

Additional information

Supplementary Information The online version contains supplementary material available at https://doi.org/10.1038/s41598-024-82938-y.

Correspondence and requests for materials should be addressed to L.L.

Reprints and permissions information is available at www.nature.com/reprints.

Publisher's note Springer Nature remains neutral with regard to jurisdictional claims in published maps and institutional affiliations.